Atmos. Chem. Phys. Discuss., 15, 35117–35155, 2015
www.atmos-chem-phys-discuss.net/15/35117/2015/
doi:10.5194/acpd-15-35117-2015

Atmospheric Chemistry and Physics
Discussions
Open Access

Aerosol source apportionment from 1 year measurements at the CESAR tower at Cabauw, NL

P. Schlag[1,2], A. Kiendler-Scharr[2], M. J. Blom[3], F. Canonaco[4], J. S. Henzing[5], M. M. Moerman[5], A. S. H. Prévôt[4], and R. Holzinger[1]

[1]Institute for Marine and Atmospheric Research Utrecht (IMAU), Utrecht University, Utrecht, the Netherlands
[2]Institute for Energy and Climate Research (IEK-8): Troposphere, Forschungszentrum Jülich, Jülich, 52425, Germany
[3]Energy Research Centre of the Netherlands (ECN), Petten, the Netherlands
[4]Laboratory of Atmospheric Chemistry, Paul Scherrer Institute (PSI), Villigen, Switzerland
[5]Netherlands Organisation for Applied Scientific Research (TNO), Utrecht, the Netherlands

Received: 10 November 2015 – Accepted: 11 November 2015
– Published: 15 December 2015

Correspondence to: P. Schlag (p.schlag@fz-juelich.de)

Published by Copernicus Publications on behalf of the European Geosciences Union.

Abstract

Intensive measurements of submicron aerosol particles and their chemical composition were performed with an Aerosol Chemical Speciation Monitor (ACSM) at the Cabauw Experimental Site for Atmospheric Research (CESAR) in Cabauw, NL. The campaign lasted nearly one year from July 2012 to June 2013 as part of the ACTRIS project. Including black carbon data an average particulate mass concentration of 9.50 $\mu g\, m^{-3}$ was obtained during the whole campaign with dominant contributions from ammonium nitrate (45 %), organic aerosol (OA, 29 %), and ammonium sulfate (19 %). 12 exceedances of the World Health Organization (WHO) $PM_{2.5}$ daily mean limit (25 $\mu g\, m^{-3}$) were observed at this rural site using PM_1 instrumentation only. Ammonium nitrate and OA represented the largest contributors to total particulate matter during periods of exceedance.

Source apportionment of OA was performed season-wise by Positive Matrix Factorization (PMF) using the Multilinear Engine 2 (ME-2) controlled via the source finder (SoFi). Primary organic aerosols were attributed mainly to traffic (8–16 % contribution to total OA, averaged season-wise) and biomass burning (0–23 %). Secondary organic aerosols (SOA, 61–84 %) dominated the organic fraction during the whole campaign, particularly on days with high mass loadings. A SOA factor which is attributed to humic-like substances (HULIS) was identified as a highly oxidized background aerosol in Cabauw. This shows the importance of atmospheric ageing processes for aerosol concentration at this rural site. Due to the large secondary fraction, the reduction of particulate mass at this rural site is challenging on a local scale.

1 Introduction

Atmospheric aerosols have large impacts on the climate directly by scattering and absorbing short wave radiation. Besides the resulting influence on the visibility (Ramanathan et al., 2007; Romanou et al., 2007), this can have a cooling or heating effect

ACPD
15, 35117–35155, 2015

Aerosol source apportionment from 1 year measurements at the CESAR tower at Cabauw, NL

P. Schlag et al.

on the atmosphere (IPCC, 2013). The indirect effect refers to the impact of particles on cloud formation and their properties.

In addition, particles can impact adversely on human health by e.g. increasing the probability of cardiopulmonary and lung cancer mortality (Pope et al., 2002). The World Health Organization (WHO) recently estimated that globally, 3.7 million deaths were attributable to ambient air pollution in both cities and rural areas in 2012 (WHO, 2014). This mortality is reported to be due to exposure to small particulate matter (PM_{10}), which can cause cardiovascular and respiratory disease, and cancers. Therefore, a number of institutions established several air quality standards for different particle sizes to limit aerosol mass. The WHO air quality guideline (global update 2005, WHO, 2006) defines a $PM_{2.5}$ daily mean limit of $25\,\mu g\,m^{-3}$ and a $PM_{2.5}$ annual mean limit of $10\,\mu g\,m^{-3}$.

Air quality and climate effects are not only depending on the particle number concentration and size, but also on their chemical composition. This information is not only relevant to investigate the nature and magnitude of each effect, but also for the identification and quantification of aerosol sources and mitigation strategies for a potential reduction of aerosol mass concentrations. Major inorganic components of PM_1 consist mainly of ammonium nitrate (NH_4NO_3) and ammonium sulfate ($(NH_4)_2SO_4$), formed in the presence of ammonia (NH_3), nitrogen oxides ($NO_x = NO + NO_2$) and sulfur dioxide (SO_2), respectively (Seinfeld and Pandis, 2006). Therefore NH_4NO_3 and $(NH_4)_2SO_4$ are strongly attributed to anthropogenic sources (Finlayson-Pitts and Pitts, 2000). Since the reactions leading to inorganic aerosol happen from gaseous precursors in the atmosphere, the condensed products are considered as secondary aerosols, while primary aerosols like black carbon (BC) are emitted directly.

In contrast, organic aerosols (OA), which can also be of primary (POA) or secondary (SOA) origin, consist of up to hundreds of thousands of different molecules (Goldstein and Galbally, 2007), where SOA contributes on average 70 % to organic aerosol mass (Hallquist et al., 2009). SOA is formed by gas to particle conversion of atmospherically oxidized semi- and low-volatile organic compounds (VOC's). Guenther et al. (1995) estimated a global VOC budget in the order of 1150 Tg carbon per year. Biogenic VOC's (BVOC's) contribute approximately 90 % of total VOC, including isoprene (50 % of total BVOC's), monoterpenes (15 %), and sesquiterpenes (3 %) (Guenther et al., 2012). In turn, 10 % of emitted VOC's are of anthropogenic origin, including e.g. alkanes, alkenes, benzene and toluene.

The investigation of the aerosol composition is critical for the development of climate models, since the composition influences important particle properties. However, its determination is still challenging, especially in case of OA, which contribute significantly to atmospheric particulate matter (Jimenez et al., 2009). In fact, the lack of knowledge on particle composition is a key contribution to the large uncertainty for the determination of the total anthropogenic radiative forcing (IPCC, 2013).

The development of online aerosol mass spectrometric techniques during the last decades enhanced the possibilities to investigate aerosol chemical composition in real-time (DeCarlo et al., 2006; Jayne et al., 2000; Jimenez et al., 2003). The Aerosol Mass Spectrometer (AMS, Aerodyne Research Inc., Billerica, MA, USA) is a powerful instrument to quantitatively measure ambient aerosol chemical composition with high time and mass resolution. Due to the high amount of maintenance from skilled and trained personnel needed for continuous operating measurement campaigns using an AMS are usually not exceeding one or two months (Sun et al., 2012). Since the variation of aerosol composition is very high depending on measurement site and season (Jimenez et al., 2009), long term measurements ($\geq$ 1 year) are clearly needed. At a European level, this effort is supported by the Aerosols, Clouds and Traces gases Research InfraStructure network (ACTRIS) program that aims at pooling high-quality data from state-of-the-art instrumentation such as the Aerodyne Aerosol Chemical Speciation Monitor (ACSM). The ACSM is specially designed for long-term continuous and real-time measurements of mass concentrations and composition of non-refractory PM_1 (NR-PM_1) species (Ng et al., 2011b).

In this study, an ACSM was used to measure the submicron aerosol chemical composition from 11 July 2012 to 3 June 2013 at the CESAR tower in Cabauw, NL, as part of the ACTRIS project. A collocated Multi-Angle Absorption Photometer (MAAP, Thermo Scientific Model 5012) provided black carbon (BC) data. Organic aerosol data was further analyzed by Positive Matrix Factorization using the Multilinear Engine 2 (Paatero, 1999) via the source finder (SoFi, Canonaco et al., 2013). This data set shows the long-term variability of particle composition and is used for source apportionment of atmospheric aerosols at this North Western European rural site, with the focus on periods where air quality standards were violated. This information can be further used to establish strategies for the reduction of particulate matter.

2 Methodology

2.1 Site description: CESAR

The CESAR tower is 220 m high and managed and operated by the Royal Netherlands Meteorological Institute (KNMI, the Netherlands). It is located in a rural site (51.970° N, 4.926° E) near Cabauw, the Netherlands, about 20 km south-west of the city of Utrecht and about 45 km south east of the Dutch North Sea cost. The site conditions are typical for North Western Europe. They can either be maritime or continental, depending on the wind direction. The surface elevation changes in the surrounding are at most a few meters over 20 km. The tower ground is approximately 0.7 m below sea level, the diurnal variation of the temperature is relatively stable (Vermeulen et al., 2011). The direct surroundings of the tower have a relatively low population density. The nearby region is used mainly by agriculture, with a mixture of intensively and extensively managed grassland. These are used also for animal keepings like cattle and sheep, besides nearby located chicken farms.

The tower is equipped with external platforms and booms at 2, 10, 20, 40, 80, 140, and 200 m. At all these levels, meteorological observations of standard parameters like wind speed, wind direction, dew point temperature, and ambient temperature are routinely performed (Ulden and Wieringa, 1996). These data sets are available at the

ACPD
15, 35117–35155, 2015

CESAR data base (KNMI, 2013). In addition, other meteorological data like precipitation, radiation and remote sensing are acquired at the tower and submitted to the CESAR data base. Also concentrations of gaseous compounds, including greenhouse gases, are monitored at CESAR (Russchenberg et al., 2005; Vermeulen et al., 2011). The National Institute for Public Health and the Environment (RIVM, the Netherlands) provides hourly data from gaseous CO, NO, NO_2, SO, SO_2, and O_3, but also daily PM_{10} measurements. Data of ambient CO_2, CH_4 (both measured at 20, 60, 120, and 200 m height), and Radon 222 (^{222}Rn, measured at 20 and 200 m height) is determined by ECN on a time scale of 30 min. A picture of the tower as well as a map indicating the land use of the Netherlands is given in the Supplement (Fig. S1).

2.2 ACSM sampling and data analysis

The ACSM measures the chemical composition of the Non-Refractory fraction of PM_1 (NR-PM_1), including the organic fraction (Org), ammonium (NH_4), nitrate (NO_3), sulfate (SO_4), and chloride (Chl), using mass spectrometric information on a time base of approximately 30 min. Recent studies showed good agreements of ACSM data with data from other aerosol instruments like the High Resolution Time-of-Flight AMS (HR-ToF-AMS) in ambient measurement campaigns, even in highly polluted areas such as Beijing (Sun et al., 2012, 2011). An intercomparison of two collocated ACSM's resulted in strong correlations ($R^2 = 0.8$) and agreements within 27 % (Budisulistiorini et al., 2014). Crenn et al. (2015) and Fröhlich et al. (2015) reported similar results from the intercomparison of 13 ACSM's, a ToF-ACSM's, a ToF-AMS, and other collocated instruments in the region of Paris, France. There, the same ACSM instrument (S/N A140-145) as the one used for this study was tested. Those results indicate that the ACSM can be used as a suitable and cost-effective alternative to the AMS for aerosol composition measurements due to its capability of stable and reproducible operation.

The ACSM used in this work is equipped with a commercial grade Quadrupole Residual Gas Analyzer (RGA), thus it is also called a Q-ACSM. This instrument is described in detail by Ng et al. (2011b). The RGA provides unit mass resolution (UMR) mass spectra. Fractions of measured UMR signals were assigned to individual aerosol species using the fragmentation table introduced by Allan et al. (2004). Due to the automated zeroing system used for the ACSM, adjustments of the fragmentation table entries concerning interferences from air beam molecules are not needed. All ACSM data processing and analysis within this work was performed using software provided by Aerodyne Research (ACSM Local, version 1.531, ARI, 2012) within IGOR Pro version 6.2.3.

Mass calibrations were performed approximately every month and were based on determining the instrument response factor (RF) (Ng et al., 2011b) using monodisperse NH_4NO_3 (320 nm) as calibration substance and a Condensation Particle Counter (CPC, TSI 3022a) as reference instrument (Jayne et al., 2000; Jimenez et al., 2003). An average RF_{NO_3} of $2.74 \pm 0.45 \times 10^{-11}$ was obtained and used for the calculation of aerosol mass concentrations. Instead of performing a mass calibration for every aerosol species, relative ionization efficiencies (RIE's), compared to that of nitrate, were used. The RIE's of NH_4 and SO_4 were determined directly during the mass calibrations by measuring dry NH_4NO_3 and $(NH_4)_2SO_4$ particles after another. Averaged over all calibrations, a RIE_{NH_4} of 7.53 ± 0.21 and a RIE_{SO_4} of 0.81 ± 0.10 were found and used for the whole data set. Calibration results gained from this particular instrument during an intercomparison in Paris as described by Crenn et al. (2015) were within the uncertainty or only slightly different ($RF_{NO_3} = 2.34 \cdot 10^{-11}$, $RIE_{NH_4} = 6.54$, $RIE_{SO_4} = 0.62$) considering the large differences between individual instruments at the intercomparison. RIE values of 1.4 and 1.3 for organics and chloride, respectively, were taken from the literature (Alfarra et al., 2004; Canagaratna et al., 2007).

A site specific, time resolved particle collection efficiency (CE) correction algorithm (equations are given in the Supplement) was applied, which was developed by Mensah et al. (2012), using SMPS data as reference. In contrast to the commonly used constant value of 0.5 or an algorithm published by Middlebrook et al. (2012), this CE correction accounts for the high ammonium nitrate mass fraction found at this site and is thus more suitable for the data presented here. According to Ng et al. (2011b) and

Sun et al. (2012), the variability of the instrument performance was corrected based on the inlet pressure and N_2 signal, as well as the signals deriving from the internal naphthalene source were taken to correct for the mass dependent ion transmission efficiency of the RGA.

The detection limits for each species were not determined within this work, but are reported to be 0.148, 0.284, 0.012, 0.024, and 0.011 $\mu g\,m^{-3}$ (3σ) for organics, ammonium, nitrate, sulfate, and chloride, respectively, at an averaging time of 30 min (Ng et al., 2011b).

During the whole campaign, the ACSM was located inside the CESAR tower building. Its inlet was placed on the roof of the building at approximately 5 m height above ground. The inlet head was equipped with a $PM_{2.5}$ cyclone (URG-2000-30EN, URG Corporation, Chapel Hill, USA). The sample air was pulled through a 10 m copper line (ID = 6.5 mm) at a flow rate of 9 $L\,min^{-1}$. From this flow, a subsample of 1 $L\,min^{-1}$ was diverted to a Nafion dryer (RH < 40 %) of which approximately 80 $mL\,min^{-1}$ entered the ACSM. This resulted in a total residence time of 18 s.

2.3 Collocated aerosol measurements

Following collocated aerosol instruments were used for cross-validation of the ACSM data: (i) a Monitor for Aerosol and Gases (MARGA, Applikon Analytical BV), operated by ECN, (ii) a Scanning Mobility Particle Sizer (SMPS, TSI 3034), operated by the Netherlands Organization for Applied Scientific Research (TNO, the Netherlands), and (iii) a HR-ToF-AMS, which was operated by Forschungszentrum Juelich during the first 6 days of the ACSM campaign. In addition, BC data obtained by a MAAP instrument (TNO, the Netherlands) was included into the analysis.

The MAAP instrument has been introduced by Petzold and Schönlinner (2004) and Petzold et al. (2005) for the determination of the black carbon (BC) fraction of PM_1 particles. It measures simultaneously the radiation penetrating through and scattered back from a particle-loaded fiber filter. Here, it is assumed that BC is not vaporized at 600 °C and thus cannot be measured by the ACSM. BC can have several origins, most likely incomplete combustion of fossil fuels and biomass. The MAAP achieves a time resolution of 5 min with an uncertainty of 12 % (Petzold and Schönlinner, 2004).

The SMPS is a sequential combination of an impactor, neutralizer, Differential Mobility Analyser (DMA, TSI) and a Condensation Particle Counter (CPC, TSI) and determines the size distribution of particles in a range of 10 to 487 nm (electromobility diameter). The SMPS aerosol mass concentration was calculated from the measured volume distributions using the particle density determined by the aerosol composition information derived from the ACSM and the MAAP. Assuming spherical particles, the total density is computed by using the densities of the aerosol species, weighted by their mass fractions. Bulk densities of NH_4NO_3 (1.72 g cm^{-3}) and $(NH_4)_2SO_4$ (1.77 g cm^{-3}), and densities of 1.8 g cm^{-3} for BC (Bond and Bergstrom, 2006; Park et al., 2004) and 1.4 g cm^{-3} for organics (Hallquist et al., 2009) were taken into account. Considering its low influence on the total particle density at this site, it is acceptable to set the density for chloride to 1 g cm^{-3} (Mensah et al., 2012).

During the presented campaign, the MAAP and the SMPS were connected to the common aerosol inlet which sampled at 60 m height. This inlet consisted of four PM_{10} size selective heads at the top, followed by a Nafion dryer to keep the relative humidity (RH) of the sample air below 40 %. The stainless steel pipe, ranging from the aperture at 60 m to the basement, has an inner diameter of 0.5" (= 1.27 cm) and ends in a manifold, where the sampled air is distributed to a variety of different instruments, including the MAAP and the SMPS, each with its own sample flow. An overall sample flow of 60 L min^{-1} was adjusted inside the 60 m pipe, assuring laminar conditions.

Recent investigations showed that aerosol measurements through this 60 m sampling line underestimate most aerosol species by approximately 33 % with an uncertainty of 10 %, mainly due to losses by Brownian diffusion to the walls and, with less importance, evaporation (J. S. Henzing, personal communication, 2014). Therefore, aerosol species and total masses obtained from this sampling line are divided by a factor of 0.66 to account for these losses. This was done for all data derived from the MAAP and SMPS.

The MARGA measures water soluble components of both the gas and aerosol phase simultaneously, including the aerosol species nitrate, ammonium, sulfate, and chloride. It uses a Wet Annular Denuder (WAD) followed by a Steam Jet Aerosol Collector (SJAC). The operational and calibration procedures, as well as details of the data analysis are given by Trebs et al. (2004). During the campaign the MARGA collected alternately the PM_1 and $PM_{2.5}$ fraction of ambient particles at ambient RH and temperature, each fraction sampled hourly with a measurement error smaller than 10 % (Schaap et al., 2011). The detection limits for the most abundant aerosol species were 0.05, 0.10, 0.08, 0.01 $\mu g\,m^{-3}$ (4σ, Rumsey et al., 2014) for ammonium, nitrate, sulfate, and chloride, respectively.

The MARGA inlet was equipped with a PM_{10} size selective head (Rupprecht and Pataschnick, R&P), placed on the roof of the tower building next to the ACSM inlet aperture at 5 m height. The sample air was transferred into the instrument within a polyethylene ("Polyflo") tube with an inner diameter of 0.5" (= 1.27 cm) and a sample flow of 16.7 L min^{-1}, which is either directed through a PM_1 or a $PM_{2.5}$ size selective head. To compare with the ACSM, only MARGA data containing PM_1 composition is considered within this work.

An Aerodyne HR-ToF-AMS was connected to the MARGA inlet during the first 6 days of the campaign. As the ACSM is built upon AMS, the latter measures likewise the chemical composition of the PM_1 non-refractory fraction. Instrumental details are available in Jayne et al. (2000), Jimenez et al. (2003), and DeCarlo et al. (2006).

2.4 Statistical methods of organic aerosol data analysis

Source apportionment of organic aerosol components were performed using Positive Matrix Factorization (PMF, Paatero, 1997; Paatero and Tapper, 1994) via the ME-2 solver (Paatero, 1999). PMF is a bilinear model and assumes that the original data set, containing variable mass spectra over time, is a linear combination of a given number of factors, each with a constant mass spectrum and its contributions over time. It has been successfully used in AMS ambient studies apportioning the measured organic mass

ACPD
15, 35117–35155, 2015

Aerosol source apportionment from 1 year measurements at the CESAR tower at Cabauw, NL

P. Schlag et al.

spectra in terms of source/process-related components (Zhang et al., 2011). With the ME-2 solver it is possible to introduce a priori mass spectral information and hence to reduce the rotational ambiguity, i.e. similar PMF results with the same goodness of fit, of PMF solutions (Paatero and Hopke, 2003).

The extraction of OA data and error matrices as mass concentrations in $\mu g\ m^{-3}$ over time, as well as their preparation for PMF/ME-2 according to Ulbrich et al. (2009), was done within the ACSM software. Only m/z's ≤ 100 were considered here since they represented nearly the whole OA mass (around 98 %) and did not interfere with ion fragments originating from naphthalene (e.g., m/z 127, 128, and 129, see also Sect. 2.2). From these matrices, the m/z 12 was discarded because it showed negative signals, probably due to too short delay time of the quadrupole scan (125 ms) after a valve switch (Fröhlich et al., 2015). In addition, the m/z's 37 and 38 were also removed from the organic matrices of the whole campaign except for winter 2013. This was done because the signal at these masses showed high interferences with the chloride isotopes ^{37}Cl and ^{38}Cl. Including these ions lead to unreasonable PMF factors which mainly contained only these two masses and represented the chloride time series, whereas during Winter 2013 no such interferences were observed.

The interface source finder (SoFi, Canonaco et al., 2013), version 4.8, was used to control ME-2 for the PMF runs of the ACSM OA data adopting the source apportionment strategy developed by Crippa et al. (2014). Briefly, unconstrained PMF runs were first investigated with 1 to 10 factors and a moderate number of seeds (10 to 15) for each factor number. If primary organic aerosol (POA) factor profiles like hydrocarbon-like OA (HOA) or OA from biomass burning (BBOA) were found, site specific POA mass spectra or spectra derived from the data base were constrained and a sensitivity analysis performed on the tightness of constraint (a value, Lanz et al., 2008). Since aged OA (or oxidized OA, OOA) factors show more variability between measurement sites in terms of their mass spectra (MS) than POA, it is not appropriate to constrain SOA factor profiles using reference spectra derived from different locations (Canonaco et al., 2015). According to Crippa et al. (2014), HOA MS should be more constrained

ACPD
15, 35117–35155, 2015

(*a* value between 0 and 0.2) than BBOA MS (a ≈ 0.3), since the BBOA fingerprint shows higher variations depending on the burning type and conditions (Alfarra et al., 2007). In each step, either in unconstrained or constrained approaches, the following criteria for finding a proper solution were used based on the recommendations from Ulbrich et al. (2009) and Canonaco et al. (2013):

- The quality parameter Q/Q_{exp} was minimized.
- Factor profiles have reasonable mass spectra, as expected for the measurement site.
- Factor time series have high correlations with respective external data sets such as gaseous CO, CO_2, NO_x, and particulate nitrate, sulfate and black carbon.
- When a proper solution is found, 50 seed runs were used to find the global minimum for Q/Q_{exp}.
- Investigation of the rotational ambiguity of the solution space is carried out using the *a* value approach for the constrained factor profiles

3 Results and discussion

3.1 Aerosol chemical composition

A meteorological overview of this campaign, including wind direction, precipitation, Radon-222 measurements and ambient temperature and relative humidity (RH) is provided in Fig. S2 in the Supplement. Table S1 in the Supplement shows temperature and RH values averaged over selected periods (see below). If not stated else, all data shown in this chapter is in UTC (local time minus 1 or 2 h, respectively) and averaged and synchronized to the ACSM data resolution of 30 min. Summing up the ACSM and MAAP data, a total mass concentration of 9.5 $\mu g\,m^{-3}$ was measured on average, with a maximum of 78.4 $\mu g\,m^{-3}$ and a minimum of 0.2 $\mu g\,m^{-3}$.

ACPD
15, 35117–35155, 2015

Data coverage of 75 % for one day and 90 % for one calendar year, respectively, is defined mandatory for a proper risk assessment according to the WHO air quality guideline. The last requirement could not be achieved either with the ACSM or with the MARGA between July 2012 and June 2013 (70 and 71 % coverage, respectively). Nevertheless, the average total mass derived from the combination of the MARGA $PM_{2.5}$ data (including all water soluble inorganic components NO_3, NH_4, SO_4, Cl, HNO_2, HNO_3, SO_2, HCl, Na, K, Mg, and Ca), MAAP PM_1-BC and ACSM PM_1 organics resulted in 13.9 $\mu g\,m^{-3}$ during this time, clearly exceeding the WHO $PM_{2.5}$ annual mean limit (25 $\mu g\,m^{-3}$) by nearly 40 %. Even when only considering the ACSM + MAAP PM_1 concentration, where a campaign average of 9.5 $\mu g\,m^{-3}$ was determined, the WHO $PM_{2.5}$ limit was approximated.

The time series of the daily mean total mass derived from both combinations (MARGA-$PM_{2.5}$+ ACSM-Org + BC and ACSM-total + BC), where the required data coverage of 75 % was reached, are shown in Fig. 1. The WHO $PM_{2.5}$ daily mean limit of 25 $\mu g\,m^{-3}$ was exceeded on 17 and 12 days, respectively. 8 and 7 exceedances were observed during a period with high pollution from 16 to 27 January 2013, respectively.

In Fig. 2 the average contributions of individual species are shown as pie charts (a) and stacked time series (b). A technical problem of the MAAP instrument was responsible for the lack of BC data from 15 February 2013 to 25 April 2013. Because of that, for further analysis the campaign was not divided strictly season-wise, but into five periods to determine properly average species contributions as shown in Fig. 2a. The first two sections represent the summer (July–August–September) and autumn (October–November–December) 2012, while the first half of 2013 was divided into periods with and without BC data. Larger gaps in ACSM data occurred mainly due to problems with the RGA detector, in addition to minor measurement gaps for maintenance and calibrations.

Overall, particulate nitrate and organics were the dominant species, representing 39 and 29 % of the total aerosol, respectively. Both compounds show similar contributions in summer (period 1) and autumn 2012 (period 2), whereas in winter (January–

ACPD
15, 35117–35155, 2015

February–March, period 3 and beginning of 4) and spring (April–May–June, periods 4 and 5) the NO_3 fraction increased up to an average of 46 % of the total particulate mass, and the organic and BC fractions decreased. The contributions of the other components showed only small variations between the seasons (see Table S2 in the Supplement.).

The most significant pollution events are highlighted in green in Fig. 2. During times with high mass concentrations (e.g. 21 to 25 October 2012, 16 to 27 January 2013, and 5 to 8 May 2013), northerly and north-easterly winds dominated. The period 16 to 27 January 2013 showed also the lowest temperatures (average: −4 °C) with respect to the whole campaign and a temperature inversion between 2 and 40 m height in the mornings of 16 and 25 January 2013. On the other hand, no temperature inversion was seen during times when very high (> 40 $\mu g\,m^{-3}$) aerosol mass loadings were observed, even in winter times. Many sudden drops of the particulate mass can be either explained by changes in wind direction and/or precipitation events, like in case of the two latter pollution events (16 to 27 January 2013, and 5 to 8 May 2013).

Figure 3 shows the diurnal patterns of each individual species and the total particulate mass for the whole campaign. Corresponding plots with data averaged separately for the five chosen periods can be found in the Supplement (Fig. S3). Overall, NO_3 showed the largest diurnal variation, with a maximum during the night/morning hours, reflecting its nighttime production and a minimum during the day due to the volatility of NH_4NO_3. This pattern is more pronounced in the warmer periods 1 and 5. Since the majority of ammonium is originated from NH_4NO_3, NH_4 has a similar pattern to that of NO_3. SO_4, which is mainly formed photochemically during the day from gaseous SO_2, showed peaks during daytime, although its overall variation is rather low. The maxima of BC can be attributed to direct emissions from traffic (morning and evening rush hours) and biomass burning events (domestic heating in the evenings/nights). Finally, OA showed peaks at the evening hours during the colder periods and a daytime minimum during the summer. More detailed discussion of the diurnal patterns of individual OA factors is given below.

ACPD
15, 35117–35155, 2015

An ion balance of all inorganic compounds indicates that too less NH_4 was measured to neutralize all NO_3 and SO_4 to their corresponding ammonium salts. The measured NH_4 mass concentration against the predicted NH_4 from the ion balance is plotted in the Supplement (Fig. S4) and resulted in a slope of 0.83 ± 0.00. One uncertainty in deriving ion balance is introduced by the use of RIE's for the inorganic species. As shown below we consider uncertainties of RIE to be of minor importance in explaining the observed low particulate NH_4 concentration. It should be noted that for the calculation of the ion balance all measured NO_3 is considered. In addition to NH_4NO_3 organic nitrates give rise to nitrate signal in the AMS, albeit with distinct difference in relative ion abundance (Alfarra et al., 2004; Fry et al., 2011, 2009). It was not possible to distinguish the organic and inorganic nitrate fraction based on their mass spectra with the ACSM. Since a relatively high amount of particulate organic nitrates was found in previous campaigns at CESAR using an AMS (Mensah, 2011), and the region is characterized by high NH_3 emissions (Derksen et al., 2011), the potential contribution of organic nitrates to the gap in the ion balance was explored as follows.

In contrast to the ion balance from the ACSM data, MARGA PM_1 measurements during the whole campaign showed a nearly 1 : 1 correlation of measured against predicted NH_4 (slope of the linear regression line: 1.03 ± 0.00, Pearson-$R^2 = 0.97$), but with a negative offset of ca. $0.30 \pm 0.01\,\mu g\,m^{-3}$. This offset, which is at least 3 times higher than the detection limits of the MARGA, cannot be explained by including positive metal ions to the ion balance, since the sum of Mg, Na, K and Ca mass concentrations had low contribution to particulate mass (average sum: $0.08\,\mu g\,m^{-3}$). Thus, significant influence of their nitrate salts to total nitrate can be excluded. In addition, as the MARGA is measuring the water-soluble nitrate fraction, the MARGA-NO_3 can be considered to be exclusively NH_4NO_3. This assumption is acceptable, as shown by using the MARGA-NO_3 instead of the ACSM-total-NO_3 for the ion balance of ACSM data (including ACSM-SO_4, -Chl and -NH_4). In this case, the correlation of measured against predicted NH_4 resulted in a nearly 1 : 1 regression line without a significant offset (Fig. S5 in the Supplement). Therefore, the mass concentration of nitrate groups

ACPD
15, 35117–35155, 2015

associated with organic molecules (hereafter called organic nitrate or $OrgNO_3$), can be estimated by subtracting the MARGA-nitrate from the ACSM-nitrate concentration. The $OrgNO_3$ time series using this approach is plotted in Fig. S6 in the Supplement, the respective diurnal variation averaged over the whole campaign in Fig. S7 in the Supplement. An average mass fraction of 9 % was calculated for $OrgNO_3$ (average concentration: $0.43\,\mu g\,m^{-3}$) in respect to total ACSM-NO_3. The organic nitrate fraction shows a maximum concentration in the night, followed by a decrease during the day.

3.2 Cross-validation of particulate total mass and chemical species concentrations

The particle density during the ACSM campaign was determined using the chemical composition data from the ACSM and the MAAP and resulted in an average of $1.63 \pm 0.12\,g\,cm^{-3}$. The time series of the particle density is given in the Supplement. It shows a significant scattering due to the relatively low signal-to-noise ratio of the ACSM, especially during periods with low mass loadings (see Fig. S8 in the Supplement). Therefore, the campaign average of the particle density ($1.63\,g\,cm^{-3}$) was used to calculate the SMPS total mass concentration from its measured volume concentration throughout the campaign. Figures S9 and S10 in the Supplement show the time series of the SMPS mass and the combined mass concentrations measured by AMS and MAAP and the correlation plot of both data sets, respectively. Using 12275 common data points for the linear fit, a good qualitative and quantitative agreement (slope: 0.84 ± 0.00, intercept: 0.80 ± 0.05, $R^2 = 0.82$) for the whole campaign was observed, including the pollution events. These correlation results lie within the expected errors.

Since the MARGA measures routinely the water soluble aerosol compounds, data from ACSM inorganic species could be averaged and compared to corresponding MARGA PM_1 data for the whole measurement period. The temporal overlap with the collocated high resolution AMS was between 11 and 17 July 2012. The correlation parameters of individual aerosol species and respective total masses between the ACSM data and the data sets from the MARGA and AMS are given in Table 1, using 1943 and 294 common data points, respectively. The corresponding correlation graphs are shown in the Supplement (Figs. S11 and S12). Except for chloride, high qualitative correlation coefficients were achieved. Furthermore, the comparison to both total mass time evolutions shows very high qualitative and quantitative agreements. The quantitative difference to the AMS-organics is also very low, and the discrepancies in case of ammonium and nitrate are within the stated ±30 % accuracy of the AMS and ACSM (Ng et al., 2011b) and the ±10 % for the MARGA–NO_3, respectively (Makkonen et al., 2012). Similar variations were also found by Crenn et al. (2015) as well as Budisulistiorini et al. (2014). The latter reported of a comparison between two collocated ACSM's (±27 %, $R^2 = 0.21$ for Chl, $R^2 > 0.8$ for the other species) and between these ACSM's and a continuous Tapered Element Oscillating Microbalance (TEOM, $PM_{2.5}$) instrument. The underestimation of the ACSM in case of sulfate exceeding the uncertainties may arise from calibration issues. The mass calibration procedure used in this work was mainly adopted from AMS procedures which may not be directly suitable for the ACSM. The RIE of sulfate might be overestimated due to high observed background signals during the calibration using $(NH_4)_2SO_4$ particles. An overestimated RIE_{SO_4} results in underestimated mass concentrations. This would in turn explain the low SO_4 mass concentrations comparing to the MARGA and AMS. Additionally, the ACSM fragmentation table could not be adjusted for interferences of ions from different aerosol species on the same m/z, but the standard table had to be used. As mentioned in Sect. 3.1, the MARGA measured only low concentrations of Mg, Na, K and Ca. Thus, contributions of their corresponding sulfate salts, for which the ACSM is less sensitive, are negligible in this context. It should also be noted that chloride concentrations can originate from particulate organic and inorganic chloride components. For the latter, the ACSM is much less sensitive than the MARGA. In turn, the MARGA might be less sensitive to organic chlorides, as they are likely less water soluble than inorganic chlorides. These explanations would explain the low agreement between the two instruments in case of chloride.

ACPD
15, 35117–35155, 2015

Note that the MARGA $PM_{2.5}$ daily averages were considerably higher or equal to corresponding MARGA PM_1 over the whole campaign. During the pollution events mentioned above, $PM_{2.5}$ values were up to 33 % higher than PM_1. As shown in Fig. 1, the exceedances of the WHO $PM_{2.5}$ daily mean limit is even higher than when only PM_1 data is considered.

Overall, the comparison of the data measured by the ACSM and MAAP with collocated aerosol instruments showed a good reliability, precision, and in most cases a good accuracy over the whole campaign, including periods with high and low mass loadings. Therefore, the here obtained chemical composition can be used qualitatively and quantitatively for the source apportionment of aerosol components at this rural site.

3.3 Factor analysis of organic aerosols

Prior to PMF analysis, the ACSM data set was subdivided into four data sets, which were explored by PMF separately, mainly due to the operational time of the ACSM that are in the following referred as: (i) July–August–September 2012: Summer 2012, (ii) October–November–December 2012: Autumn 2012, (iii) January–February–March 2013: Winter 2013, (iv) April–May–beginning of June 2013: Spring 2013. A more detailed overview of the selected seasons is given in Table S3 in the Supplement.

Figure 4 summarizes the time series of PMF factor classes (two POA factors: HOA and BBOA; and two SOA factors: OOA and HULIS, see below for descriptions) found for all seasons, except for BBOA in Summer 2012. A corresponding graph dividing these PMF results into the five periods according to Fig. 2 is shown in Fig. S18 in the Supplement. Factor profiles including fractional contributions of marker ions (f44, f43, and f60) and diurnal variations for Winter 2013 are displayed in Fig. 5 as a representative example. Corresponding graphs for every season are shown in Figs. S13 and S14 in the Supplement, respectively. Table S4 in the Supplement gives an overview of the temporal correlations of each factor with external data sets, while scatter plots from Winter 2013 profiles against profiles found in May 2008 at CESAR by Crippa et al. (2014) are given in Fig. S15 in the Supplement.

ACPD
15, 35117–35155, 2015

As mentioned, no significant BBOA influence was seen in Summer 2012. Thus, a three-factor solution was chosen for this season and consequently, no BBOA time series exists at that time. For all other factors the time series are continuous on 1 October 2012, i.e. analysis of separate data files leads to a consistent result in terms of both factor profiles and concentrations. A single PMF analysis of the whole data set with constrained HOA and BBOA profiles with similar *a* values lead to solutions with a highly overestimated BBOA factor in the summer, compared to the results when the seasons were explored individually (see Figs. S16 and S17 in the Supplement). This behavior may result from the relatively high degree of freedom given for BBOA, which resulted in a high rotational ambiguity. As another result, the contributions of individual factors change significantly in some periods, especially for the OOA factor during pollution events. This is mainly driven by the different OOA-f_{44} and -f_{43} values.

The SOA factors showed always higher contribution (54–84 %, averaged season-wise) to total organics compared to POA (16–46 %). The POA profiles were constrained within ME-2 using the HOA and BBOA mass spectra found by ME-2 operated PMF analyses by Crippa et al. (2014) at the CESAR tower in Cabauw in March 2009. For the HOA profile, a constant *a* value of 0.1 was found to be most suitable for every season. If observed, the BBOA *a* value was set to either 0.2 (Autumn 2012) or 0.3 (Winter and Spring 2013).

For all PMF factors, no preferential wind direction was observed over the entire campaign. During the pollution events mentioned above, OOA originated mostly from the directions between 20 and 180° in respect to the tower. This is not the case for HULIS, which origins varied throughout all directions, also during pollution events.

The seasonal average HOA contribution to total organic mass was highest in Summer 2012 and lowest in Spring 2013 (16 and 8 %, respectively). All HOA diurnal patterns (Fig. 5b) showed a maximum at 7 and 11 a.m. (LT) and a slight increase in the evening, emphasizing that its main source is related to traffic likewise to BC (see Sect. 3.1). In Winter 2013, these maxima were less distinctive comparing to the other

ACPD
15, 35117–35155, 2015

seasons. Highest temporal agreements with HOA were seen by the POA tracers BC, NO_x and CO (R^2 = 0.38, 0.47, and 0.47, respectively) over the entire campaign.

The BBOA profile showed a very high contribution of m/z 60, which is dominated by the $C_2H_4O_2^+$ ion. This fragment is characteristic for anhydrosugars such as levoglucosan (Alfarra et al., 2007) which are established markers of wood combustion processes (Simoneit and Elias, 2001; Simoneit et al., 1999). The fractions of m/z 60 to the BBOA profile in Autumn 2012 (3.7 %) and Winter 2013 (3.2 %) are higher than in Spring 2013 (2.4 %). As mentioned, BBOA was not found in Summer 2012. This was verified by the fact that the contribution of m/z 60 to the BBOA profile decreases for higher a values in that season, which is an indication for the non-existence of BBOA. The highest contributions of BBOA to total organics were seen in the colder Autumn (23 %) and Winter seasons (15 %). This and the diurnal maximum during the evenings and nights match the expectations for a factor linked with domestic heating activities, together with the fact, that this factor was not seen during the warmer summer season. Averaged over the whole campaign, the contribution to total organics was 13 %, including Summer 2012, where it's fraction was set to zero. In Winter, the correlations with BC and CO were higher (R^2 = 0.64 and 0.57, respectively) than over the whole campaign (R^2 = 0.39 and 0.49, respectively), meaning that these compounds are reasonably more attributed to domestic heating during the colder periods in this region.

The OOA profile is similar to a MS pattern as expected for a low volatile OOA (LVOOA) factor. The correlation coefficients (Pearson-R^2) with the OOA and LVOOA spectra given by Ng et al. (2011a) are 0.94 and 0.97, respectively. Similar agreement was found compared to the LVOOA factor observed by Mensah (2011) and Crippa et al. (2014) (R^2 = 0.97 and 0.94, respectively) at the CESAR tower in May 2008. The OOA factor showed a night-time maximum and a day-time minimum. This is rather characteristic for a semi volatile OOA (SVOOA) behavior, as well as the high agreement with NO_3 over the whole year (R^2 = 0.63), as described by Lanz et al. (2007). The correlation to the LVOOA associated compound SO_4 is less significant (R^2 = 0.48). OOA dominated the organic fraction in Winter and Spring 2013 (47 and 48 % contribution, re-

ACPD
15, 35117–35155, 2015

Aerosol source apportionment from 1 year measurements at the CESAR tower at Cabauw, NL

P. Schlag et al.

spectively; 33 % over the whole year). During the defined pollution events the increase of the OOA mass concentration (up to 11.8 µg m^{-3}), relative to the campaign average (1.05 µg m^{-3}), is much stronger compared to the other PMF factors, demonstrating that this factor is mainly responsible the high total OA mass during these periods.

The so called HULIS factor showed the highest f_{44} values of all factors, increasing from Summer 2012 to Spring 2013 from 0.23 to 0.35. The HULIS factor class was first observed by Mensah (2011) in previous AMS campaigns at the CESAR tower in May 2008 and March 2009. The identification and characterization of this factor class was done in the 2008 campaign by the comparison with data from an ion-exchange chromatographic method for direct quantification of humic-like substances (HULIS) and from water-soluble organic carbon (WSOC) analyzed offline on a set of filters collected in parallel (Paglione et al., 2014). The HULIS factor provided the highest contribution to the total organic mass over the entire campaign (41 %) and was the dominant factor in Summer and Autumn 2012. Since it had no distinct diurnal variation and preferential wind direction, it can be considered as regional background aerosol at this rural site. Additionally, the variation between the seasonal average concentrations of HULIS within the ACSM data set is less than ±10 %. Also the comparison to the most important tracers (Table S4 in the Supplement) showed no preferential attribution, either to a low-volatile ($R^2 = 0.41$ with SO_4), semi-volatile ($R^2 = 0.47$ with NO_3) or to primary organic aerosol ($R^2 = 0.47$ with BC). These characteristics were also reported for the HULIS factor found at CESAR in May 2008 (Crippa et al., 2014; Mensah, 2011). The correlation of the sum of the secondary inorganic species NO_3 and SO_4 with the sum of the OOA and HULIS time series gives a coefficient of $R^2 = 0.70$, which is slightly higher than with OOA only ($R^2 = 0.67$). This might confirm the SOA character of the HULIS factor. The reason why HULIS was the dominant factor in Summer and Autumn 2012 is due to the lower mass concentrations of the other factors compared to the remaining periods. In turn, OA mass increased during pollution events mainly due to the increase of the other SOA factor, namely OOA. A number of studies are published with different theories on the formation and sources of atmospheric HULIS. It shows similarities to terrestrial humic acids (HA) and fulvic acids (FA) due to their (poly-)acidic nature, but with lower molecular weight (< 1000 amu) than HA or FA (Graber and Rudich, 2006; Kiss et al., 2003). On the other hand, solid-phase extraction protocols for HULIS associate them with the more hydrophobic fraction of water-soluble aerosols (e.g. Varga et al., 2001). Graber and Rudich (2006) suggested that the formation of HULIS happens by oligomerization of lighter organic acids in liquid droplets in the atmosphere within time scales of hours to days. This emphasizes, that HULIS is an ubiquitous background factor at Cabauw, characterized as regionally well mixed aerosol of long atmospheric lifetime.

3.4 Composition and sources of aerosols during pollution events

The investigation of the aerosol composition during the pollution events showed that the majority was contributed from secondary aerosols. As an example, Fig. 6 displays average abundances during two selected periods (17 to 21 August 2012 and 16 to 27 January 2013), where the organic fraction is further distinguished into the PMF factors. Nitrate and organics are still the dominant species, while the POA components (BC, HOA, BBOA) have even less influence than averaged over the respective season. An exception is seen from BBOA, which contribution is reasonably higher during the latter pollution event with very low temperatures, when domestic heating sources most likely increased. But even at this time, primary organics do not exceed 11 % of total mass on average.

Since the major inorganic components NH_4NO_3 and $(NH_4)_2SO_4$ are produced by atmospheric processes, they are considered as secondary aerosols. Together with the high abundance of SOA (OOA, HULIS), chemically aged aerosol components have the largest impact on total particulate mass (up to 90 %) at Cabauw. The largest effect on a potential reduction of particulate mass can therefore be achieved by reducing NO_x and/or NH_3 emissions, the anthropogenic precursors of particulate NH_4 and NO_3. Indeed, on 16 January 2013 highest NO_x values were observed compared to the whole campaign (daily mean: 96 $\mu g\,m^{-3}$; seasonal average: 29 $\mu g\,m^{-3}$). Also the

ACPD
15, 35117–35155, 2015

highest NH_3 values were obtained between 17 and 19 August 2012 (daily means: 26–28 µg m^{-3}; seasonal average: 10 µg m^{-3}). These ammonia values are higher than previously reported for Cabauw, e.g. by Derksen et al. (2011) in May 2008 (approximately 20 µg m^{-3}). Lolkema et al. (2015) gave an annual average of 5.3 µg m^{-3} for 2013 in this region.

As indicated by model results for the South Western United States from Zhang and Wu (2013), the reduction of NH_3 emissions, in conjunction with already implemented SO_2 and NO_x emission reductions, can further reduce $PM_{2.5}$ than reducing SO_2 and NO_x emissions alone, particularly for regions with high emissions of NH_3 from agricultural sources. The latter is clearly the case for Cabauw with its high number of animal husbandry and the use of nitrogen containing fertilizers around the CESAR tower. Banzhaf et al. (2013) derived similar conclusions for PM_{10} using different emission scenarios within domains covering Germany and Europe. Finally, Megaritis et al. (2014) calculated by applying a 3-D chemical transport model over Europe that a reduction of NH_3 emissions by 50 % would have a much higher effect on reducing $PM_{2.5}$ than decreasing NO_x emissions by 50 %. The latter scenario would result in higher tropospheric ozone concentrations especially in summer terms (4 % over Western Europe and up to 40 % in major urban areas) and higher amounts of particulate sulfate and OA by 8 and 12 %, respectively, in winter.

4 Conclusions

This work provides chemical composition data of atmospheric aerosols acquired during one year at the CESAR tower in Cabauw, the Netherlands, which is a representative rural site for North Western Europe. The concentration of submicron particles from combined ACSM and MAAP data showed 12 exceedances from the WHO $PM_{2.5}$ daily mean limit. The respective campaign average of 9.5 µg m^{-3} approached the WHO $PM_{2.5}$ annual mean limit. These findings were confirmed by collocated aerosol instruments.

ACPD
15, 35117–35155, 2015

Particulate mass loadings found at this rural site are most likely determined by atmospheric chemistry in the gas phase and particle phase aging. It is shown that the reduction of gaseous ammonia emissions is essential to reduce PM_1 concentrations in Cabauw, as it would reduce especially the particulate ammonium nitrate, which is the major aerosol component (39 % on average) and representing the more hygroscopic fraction.

The local mitigation of organic aerosol mass (29 % contribution on average) is more challenging, as secondary organic aerosols are highly abundant at this site (74 and 22 % of OA and total PM_1 on average, respectively) and the presented data set shows no designated local source of the ubiquitous HULIS fraction. In turn, primary organic aerosols emitted mainly from traffic and biomass burning (12 and 13 % of OA on average) have only minor importance. For a more detailed identification of the SOA sources compound specific measurements of OA as well as routine VOC monitoring are needed.

The Supplement related to this article is available online at doi:10.5194/acpd-15-35117-2015-supplement.

Acknowledgements. The research leading to these results has received funding from the European Union Seventh Framework Programme (FP7/2007-2013) under grant agreement no. 262254. We appreciate the support from KNMI in hosting the experiment at Cabauw and for the access to meteorological data from the tower. The authors thank the CESAR tower team for the big support during the campaign, as well as RIVM for providing CO, NO_x, and O_3 data. Additionally, the authors appreciate measurements of ambient CO_2 and Radon 222 (^{222}Rn) done by ECN. We also thank Philip Croteau (PSI) for his support during the measurements regarding the data acquisition and evaluation.

The article processing charges for this open-access publication were covered by a Research Centre of the Helmholtz Association.

ACPD
15, 35117–35155, 2015

References

Alfarra, M. R., Coe, H., Allan, J. D., Bower, K. N., Boudries, H., Canagaratna, M. R., Jimenez, J. L., Jayne, J. T., Garforth, A. A., Li, S.-M., and Worsnop, D. R.: Characterization of urban and rural organic particulate in the Lower Fraser Valley using two aerodyne aerosol mass spectrometers, Atmos. Environ., 38, 5745–5758, 2004.

Alfarra, M. R., Prevot, A. S. H., Szidat, S., Sandradewi, J., Weimer, S., Lanz, V. A., Schreiber, D., Mohr, M., and Baltensperger, U.: Identification of the mass spectral signature of organic aerosols from wood burning emissions, Envir. Sci. Tech. Lib., 41, 5770–5777, 2007.

Allan, J. D., Delia, A. E., Coe, H., Bower, K. N., Alfarra, M. R., Jimenez, J. L., Middlebrook, A. M., Drewnick, F., Onasch, T. B., Canagaratna, M. R., Jayne, J. T., and Worsnop, D. R.: A generalised method for the extraction of chemically resolved mass spectra from Aerodyne Aerosol Mass Spectrometer data, J. Aerosol Sci., 35, 909–922, 2004.

ARI: Aerosol Chemical Speciation Monitor official webpage. Aerodyne Research, Inc., available at: https://sites.google.com/site/ariacsm/ (last access: 5 May 2014), 2012.

Banzhaf, S., Schaap, M., Wichink Kruit, R. J., Denier van der Gon, H. A. C., Stern, R., and Builtjes, P. J. H.: Impact of emission changes on secondary inorganic aerosol episodes across Germany, Atmos. Chem. Phys., 13, 11675–11693, doi:10.5194/acp-13-11675-2013, 2013.

Bond, T. C. and Bergstrom, R. W.: Light absorption by carbonaceous particles: an investigative review, Aerosol Sci. Tech., 40, 27–67, 2006.

Budisulistiorini, S. H., Canagaratna, M. R., Croteau, P. L., Baumann, K., Edgerton, E. S., Kollman, M. S., Ng, N. L., Verma, V., Shaw, S. L., Knipping, E. M., Worsnop, D. R., Jayne, J. T., Weber, R. J., and Surratt, J. D.: Intercomparison of an aerosol chemical speciation monitor (ACSM) with ambient fine aerosol measurements in downtown Atlanta, Georgia, Atmos. Meas. Tech., 7, 1929–1941, 2014, http://www.atmos-meas-tech.net/7/1929/2014/.

Canagaratna, M. R., Jayne, J. T., Jimenez, J. L., Allan, J. D., Alfarra, M. R., Zhang, Q., Onasch, T. B., Drewnick, F., Coe, H., Middlebrook, A., Delia, A., Williams, L. R., Trimborn, A. M., Northway, M. J., DeCarlo, P. F., Kolb, C. E., Davidovits, P., and Worsnop, D. R.: Chemical and microphysical characterization of ambient aerosols with the Aerodyne Aerosol Mass Spectrometer, Mass Spectrom. Rev., 26, 185–222, 2007.

Canonaco, F., Crippa, M., Slowik, J. G., Baltensperger, U., and Prévôt, A. S. H.: SoFi, an IGOR-based interface for the efficient use of the generalized multilinear engine (ME-2) for the source apportionment: ME-2 application to aerosol mass spectrometer data, Atmos. Meas. Tech., 6, 3649–3661, doi:10.5194/amt-6-3649-2013, 2013.

Canonaco, F., Slowik, J. G., Baltensperger, U., and Prévôt, A. S. H.: Seasonal differences in oxygenated organic aerosol composition: implications for emissions sources and factor analysis, Atmos. Chem. Phys., 15, 6993–7002, doi:10.5194/acp-15-6993-2015, 2015.

Crenn, V., Sciare, J., Croteau, P. L., Verlhac, S., Fröhlich, R., Belis, C. A., Aas, W., Äijälä, M., Alastuey, A., Artiñano, B., Baisnée, D., Bonnaire, N., Bressi, M., Canagaratna, M., Canonaco, F., Carbone, C., Cavalli, F., Coz, E., Cubison, M. J., Esser-Gietl, J. K., Green, D. C., Gros, V., Heikkinen, L., Herrmann, H., Lunder, C., Minguillón, M. C., Močnik, G., O'Dowd, C. D., Ovadnevaite, J., Petit, J.-E., Petralia, E., Poulain, L., Priestman, M., Riffault, V., Ripoll, A., Sarda-Estève, R., Slowik, J. G., Setyan, A., Wiedensohler, A., Baltensperger, U., Prévôt, A. S. H., Jayne, J. T., and Favez, O.: ACTRIS ACSM intercomparison – Part I: Reproducibility of concentration and fragment results from 13 individual Quadrupole Aerosol Chemical Speciation Monitors (Q-ACSM) and consistency with Time-of-Flight ACSM (ToF-ACSM), High Resolution ToF Aerosol Mass Spectrometer (HR-ToF-AMS) and other co-located instruments, Atmos. Meas. Tech. Discuss., 8, 7239–7302, doi:10.5194/amtd-8-7239-2015, 2015.

Crippa, M., Canonaco, F., Lanz, V. A., Äijälä, M., Allan, J. D., Carbone, S., Capes, G., Ceburnis, D., Dall'Osto, M., Day, D. A., DeCarlo, P. F., Ehn, M., Eriksson, A., Freney, E., Hildebrandt Ruiz, L., Hillamo, R., Jimenez, J. L., Junninen, H., Kiendler-Scharr, A., Kortelainen, A.-M., Kulmala, M., Laaksonen, A., Mensah, A. A., Mohr, C., Nemitz, E., O'Dowd, C., Ovadnevaite, J., Pandis, S. N., Petäjä, T., Poulain, L., Saarikoski, S., Sellegri, K., Swietlicki, E., Tiitta, P., Worsnop, D. R., Baltensperger, U., and Prévôt, A. S. H.: Organic aerosol components derived from 25 AMS data sets across Europe using a consistent ME-2 based source apportionment approach, Atmos. Chem. Phys., 14, 6159–6176, doi:10.5194/acp-14-6159-2014, 2014.

DeCarlo, P. F., Kimmel, J. R., Trimborn, A., Northway, M. J., Jayne, J. T., Aiken, A. C., Gonin, M., Fuhrer, K., Horvath, T., Docherty, K. S., Worsnop, D. R., and Jimenez, J. L.: Field-deployable, High-Resolution, Time-of-Flight Aerosol Mass Spectrometer, Anal. Chem., 78, 8281–8289, 2006.

Derksen, J. W. B., Roelofs, G.-J. H., Otjes, R., de Leeuw, G., and Röckmann, T.: Impact of ammonium nitrate chemistry on the AOT in Cabauw, the Netherlands, Atmos. Environ., 45, 5640–5646, 2011.

Finlayson-Pitts, B. J. and Pitts, J. N.: Chemistry of the upper and lower atmosphere - theory, experiments and applications, Academic Press, 2000.
Fröhlich, R., Crenn, V., Setyan, A., Belis, C. A., Canonaco, F., Favez, O., Riffault, V., Slowik, J. G., Aas, W., Aijälä, M., Alastuey, A., Artiñano, B., Bonnaire, N., Bozzetti, C., Bressi, M., Carbone, C., Coz, E., Croteau, P. L., Cubison, M. J., Esser-Gietl, J. K., Green, D. C., Gros, V., Heikkinen, L., Herrmann, H., Jayne, J. T., Lunder, C. R., Minguillón, M. C., Močnik, G., O'Dowd, C. D., Ovadnevaite, J., Petralia, E., Poulain, L., Priestman, M., Ripoll, A., Sarda-Estève, R., Wiedensohler, A., Baltensperger, U., Sciare, J., and Prévôt, A. S. H.: ACTRIS ACSM intercomparison – Part 2: Intercomparison of ME-2 organic source apportionment results from 15 individual, co-located aerosol mass spectrometers, Atmos. Meas. Tech., 8, 2555–2576, doi:10.5194/amt-8-2555-2015, 2015.
Fry, J. L., Kiendler-Scharr, A., Rollins, A. W., Wooldridge, P. J., Brown, S. S., Fuchs, H., Dubé, W., Mensah, A., dal Maso, M., Tillmann, R., Dorn, H.-P., Brauers, T., and Cohen, R. C.: Organic nitrate and secondary organic aerosol yield from NO_3 oxidation of β-pinene evaluated using a gas-phase kinetics/aerosol partitioning model, Atmos. Chem. Phys., 9, 1431–1449, doi:10.5194/acp-9-1431-2009, 2009.
Fry, J. L., Kiendler-Scharr, A., Rollins, A. W., Brauers, T., Brown, S. S., Dorn, H.-P., Dubé, W. P., Fuchs, H., Mensah, A., Rohrer, F., Tillmann, R., Wahner, A., Wooldridge, P. J., and Cohen, R. C.: SOA from limonene: role of NO_3 in its generation and degradation, Atmos. Chem. Phys., 11, 3879–3894, doi:10.5194/acp-11-3879-2011, 2011.
Goldstein, A. H. and Galbally, I. E.: Known and unexplored organic constituents in the earth's atmosphere, Envir. Sci. Tech. Lib., 41, 1514-1521, 2007.
Graber, E. R. and Rudich, Y.: Atmospheric HULIS: How humic-like are they? A comprehensive and critical review, Atmos. Chem. Phys., 6, 729–753, doi:10.5194/acp-6-729-2006, 2006.
Guenther, A., Hewitt, C. N., Erickson, D., Fall, R., Geron, C., Graedel, T., Harley, P., Klinger, L., Lerdau, M., Mckay, W. A., Pierce, T., Scholes, B., Steinbrecher, R., Tallamraju, R., Taylor, J., and Zimmerman, P.: A global model of natural volatile organic compound emissions, J. Geophys. Res.-Atmos., 100, 8873–8892, 1995.
Guenther, A. B., Jiang, X., Heald, C. L., Sakulyanontvittaya, T., Duhl, T., Emmons, L. K., and Wang, X.: The Model of Emissions of Gases and Aerosols from Nature version 2.1 (MEGAN2.1): an extended and updated framework for modeling biogenic emissions, Geosci. Model Dev., 5, 1471–1492, doi:10.5194/gmd-5-1471-2012, 2012.

Hallquist, M., Wenger, J. C., Baltensperger, U., Rudich, Y., Simpson, D., Claeys, M., Dommen, J., Donahue, N. M., George, C., Goldstein, A. H., Hamilton, J. F., Herrmann, H., Hoffmann, T., Iinuma, Y., Jang, M., Jenkin, M., Jimenez, J. L., Kiendler-Scharr, A., Maenhaut, W., McFiggans, G., Mentel, T. F., Monod, A., Prevot, A. S. H., Seinfeld, J. H., Surratt, J. D., Szmigielski, R., and Wildt, J.: The formation, properties and impact of secondary organic aerosol: current and emerging issues, Atmos. Chem. Phys., 9, 3555–3762, 2009, http://www.atmos-chem-phys.net/9/3555/2009/.

IPCC: Climate Change 2013: The Physical Science Basis. Contribution of Working Group I to the Fifth Assessment Report of the Intergovernmental Panel on Climate Change. Cambridge University Press, Cambridge, United Kingdom and New York, NY, USA, 2013.

Jayne, J. T., Leard, D. C., Zhang, X. F., Davidovits, P., Smith, K. A., Kolb, C. E., and Worsnop, D. R.: Development of an Aerosol Mass Spectrometer for size and composition analysis of submicron particles, Aerosol Sci. Tech., 33, 49–70, 2000.

Jimenez, J. L., Jayne, J. T., Shi, Q., Kolb, C. E., Worsnop, D. R., Yourshaw, I., Seinfeld, J. H., Flagan, R. C., Zhang, X., Smith, K. A., Morris, J. W., and Davidovits, P.: Ambient aerosol sampling using the aerodyne aerosol mass spectrometer, J. Geophys. Res.-Atmos., 108, 2003.

Jimenez, J. L., Canagaratna, M. R., Donahue, N. M., Prevot, A. S. H., Zhang, Q., Kroll, J. H., DeCarlo, P. F., Allan, J. D., Coe, H., Ng, N. L., Aiken, A. C., Docherty, K. S., Ulbrich, I. M., Grieshop, A. P., Robinson, A. L., Duplissy, J., Smith, J. D., Wilson, K. R., Lanz, V. A., Hueglin, C., Sun, Y. L., Tian, J., Laaksonen, A., Raatikainen, T., Rautiainen, J., Vaattovaara, P., Ehn, M., Kulmala, M., Tomlinson, J. M., Collins, D. R., Cubison, M. J., Dunlea, E. J., Huffman, J. A., Onasch, T. B., Alfarra, M. R., Williams, P. I., Bower, K., Kondo, Y., Schneider, J., Drewnick, F., Borrmann, S., Weimer, S., Demerjian, K., Salcedo, D., Cottrell, L., Griffin, R., Takami, A., Miyoshi, T., Hatakeyama, S., Shimono, A., Sun, J. Y., Zhang, Y. M., Dzepina, K., Kimmel, J. R., Sueper, D., Jayne, J. T., Herndon, S. C., Trimborn, A. M., Williams, L. R., Wood, E. C., Middlebrook, A. M., Kolb, C. E., Baltensperger, U., and Worsnop, D. R.: Evolution of organic aerosols in the atmosphere, Science, 326, 1525–1529, 2009.

Kiss, G., Tombacz, E., Varga, B., Alsberg, T., and Persson, L.: Estimation of the average molecular weight of humic-like substances isolated from fine atmospheric aerosol, Atmos. Environ., 37, 3783–3794, 2003.

ACPD
15, 35117–35155, 2015

KNMI: Cesar Database. Royal Netherlands Meteorological Institute (KNMI, The Netherlands), available at:http://www.cesar-database.nl/ (last access: 25 April 2014), 2013.

Lanz, V. A., Alfarra, M. R., Baltensperger, U., Buchmann, B., Hueglin, C., and Prévôt, A. S. H.: Source apportionment of submicron organic aerosols at an urban site by factor analytical modelling of aerosol mass spectra, Atmos. Chem. Phys., 7, 1503–1522, doi:10.5194/acp-7-1503-2007, 2007.

Lanz, V. A., Alfarra, M. R., Baltensperger, U., Buchmann, B., Hueglin, C., Szidat, S., Wehrli, M. N., Wacker, L., Weimer, S., Caseiro, A., Puxbaum, H., and Prevot, A. S. H.: Source attribution of submicron organic aerosols during wintertime inversions by advanced factor analysis of aerosol mass spectra, Environ. Sci. Technol., 42, 214–220, 2008.

Lolkema, D. E., Noordijk, H., Stolk, A. P., Hoogerbrugge, R., van Zanten, M. C., and van Pul, W. A. J.: The Measuring Ammonia in Nature (MAN) network in the Netherlands, Biogeosciences, 12, 5133–5142, doi:10.5194/bg-12-5133-2015, 2015.

Makkonen, U., Virkkula, A., Mäntykenttä, J., Hakola, H., Keronen, P., Vakkari, V., and Aalto, P. P.: Semi-continuous gas and inorganic aerosol measurements at a Finnish urban site: comparisons with filters, nitrogen in aerosol and gas phases, and aerosol acidity, Atmos. Chem. Phys., 12, 5617–5631, doi:10.5194/acp-12-5617-2012, 2012.

Megaritis, A. G., Fountoukis, C., and Pandis, S. N.: Sensitivity of fine PM levels in Europe to emissions changes, in: Air Pollution Modeling and its Application XXII, edited by: Steyn, D. G., Builtjes, P. J. H., and Timmermans, R. M. A., Springer, Netherlands, 333–338 pp., 2014.

Mensah, A. A.: Water and organic nitrate detection in an AMS: laboratory characterization and application to ambient measurements, Universität zu Köln, 2011.

Mensah, A. A., Holzinger, R., Otjes, R., Trimborn, A., Mentel, Th. F., ten Brink, H., Henzing, B., and Kiendler-Scharr, A.: Aerosol chemical composition at Cabauw, The Netherlands as observed in two intensive periods in May 2008 and March 2009, Atmos. Chem. Phys., 12, 4723–4742, doi:10.5194/acp-12-4723-2012, 2012.

Middlebrook, A. M., Bahreini, R., Jimenez, J. L., and Canagaratna, M. R.: Evaluation of composition-dependent collection efficiencies for the Aerodyne Aerosol Mass Spectrometer using field data, Aerosol Sci. Tech., 46, 258–271, 2012.

Ng, N. L., Canagaratna, M. R., Jimenez, J. L., Zhang, Q., Ulbrich, I. M., and Worsnop, D. R.: Real-time methods for estimating organic component mass concentrations from Aerosol Mass Spectrometer data, Envir. Sci. Tech. Lib., 45, 910–916, 2011a.

Ng, N. L., Herndon, S. C., Trimborn, A., Canagaratna, M. R., Croteau, P. L., Onasch, T. B., Sueper, D., Worsnop, D. R., Zhang, Q., Sun, Y. L., and Jayne, J. T.: An Aerosol Chemical Speciation Monitor (ACSM) for routine monitoring of the composition and mass concentrations of ambient aerosol, Aerosol Sci. Tech., 45, 780–794, 2011b.
Paatero, P.: Least squares formulation of robust non-negative factor analysis, Chemometr. Intell. Lab., 37, 23–35, 1997.
Paatero, P.: The multilinear engine - a table-driven, least squares program for solving multilinear problems, including the n-way parallel factor analysis model, J. Comput. Graph. Stat., 8, 854–888, 1999.
Paatero, P. and Hopke, P. K.: Discarding or downweighting high-noise variables in factor analytic models, Anal. Chim. Acta, 490, 277–289, 2003.
Paatero, P. and Tapper, U.: Positive matrix factorization - a non-negative factor model with optimal utilization of error-estimates of data values, Environmetrics, 5, 111–126, 1994.
Paglione, M., Kiendler-Scharr, A., Mensah, A. A., Finessi, E., Giulianelli, L., Sandrini, S., Facchini, M. C., Fuzzi, S., Schlag, P., Piazzalunga, A., Tagliavini, E., Henzing, J. S., and Decesari, S.: Identification of humic-like substances (HULIS) in oxygenated organic aerosols using NMR and AMS factor analyses and liquid chromatographic techniques, Atmos. Chem. Phys., 14, 25–45, doi:10.5194/acp-14-25-2014, 2014.
Park, K., Kittelson, D., Zachariah, M., and McMurry, P.: Measurement of inherent material density of nanoparticle agglomerates, J. Nanopart. Res., 6, 267–272, 2004.
Petzold, A. and Schönlinner, M.: Multi-angle absorption photometry: a new method for the measurement of aerosol light absorption and atmospheric black carbon, J. Aerosol Sci., 35, 421–441, 2004.
Petzold, A., Schloesser, H., Sheridan, P. J., Arnott, W. P., Ogren, J. A., and Virkkula, A.: Evaluation of multiangle absorption photometry for measuring aerosol light absorption, Aerosol Sci. Tech., 39, 40–51, 2005.
Pope, I. C., Burnett, R. T., and Thun, M. J.: Lung cancer, cardiopulmonary mortality, and long-term exposure to fine particulate air pollution, J. Amer. Med. Assoc., 287, 1132–1141, 2002.
Ramanathan, V., Li, F., Ramana, M. V., Praveen, P. S., Kim, D., Corrigan, C. E., Nguyen, H., Stone, E. A., Schauer, J. J., Carmichael, G. R., Adhikary, B., and Yoon, S. C.: Atmospheric brown clouds: hemispherical and regional variations in long-range transport, absorption, and radiative forcing, J. Geophys. Res.-Atmos., 112, D22S21, doi:10.1029/2006GL028356, 2007.

Romanou, A., Liepert, B., Schmidt, G. A., Rossow, W. B., Ruedy, R. A., and Zhang, Y.: 20th century changes in surface solar irradiance in simulations and observations, Geophys. Res. Lett., 34, L05713, doi:10.1029/2006JD008124, 2007.
Rumsey, I. C., Cowen, K. A., Walker, J. T., Kelly, T. J., Hanft, E. A., Mishoe, K., Rogers, C., Proost, R., Beachley, G. M., Lear, G., Frelink, T., and Otjes, R. P.: An assessment of the performance of the Monitor for AeRosols and GAses in ambient air (MARGA): a semi-continuous method for soluble compounds, Atmos. Chem. Phys., 14, 5639–5658, doi:10.5194/acp-14-5639-2014, 2014.
Russchenberg, H., Bosveld, F., Swart, D., ten Brink, H., de Leeuw, G., Uijlenhoet, R., Arbesser-Rastburg, B., van der Marel, H., Ligthart, L., Boers, R., and Apituley, A.: Ground-based atmospheric remote sensing in the Netherlands: European outlook, IEICE T. Commun., E88B, 2252–2258, 2005.
Schaap, M., Otjes, R. P., and Weijers, E. P.: Illustrating the benefit of using hourly monitoring data on secondary inorganic aerosol and its precursors for model evaluation, Atmos. Chem. Phys., 11, 11041–11053, doi:10.5194/acp-11-11041-2011, 2011.
Seinfeld, J. H. and Pandis, S. N.: Atmospheric Chemistry and Physics: From Air Pollution to Climate Change, Wiley-Interscience, Hoboken, NJ, USA, 2006.
Simoneit, B. R. T. and Elias, V. O.: Detecting organic tracers from biomass burning in the atmosphere, Mar. Pollut. Bull., 42, 805–810, 2001.
Simoneit, B. R. T., Schauer, J. J., Nolte, C. G., Oros, D. R., Elias, V. O., Fraser, M. P., Rogge, W. F., and Cass, G. R.: Levoglucosan, a tracer for cellulose in biomass burning and atmospheric particles, Atmos. Environ., 33, 173–182, 1999.
Sun, Y., Wang, Z., Dong, H., Yang, T., Li, J., Pan, X., Chen, P., and Jayne, J. T.: Characterization of summer organic and inorganic aerosols in Beijing, China with an Aerosol Chemical Speciation Monitor, Atmos. Environ., 51, 250–259, 2012.
Sun, Y.-L., Zhang, Q., Schwab, J. J., Demerjian, K. L., Chen, W.-N., Bae, M.-S., Hung, H.-M., Hogrefe, O., Frank, B., Rattigan, O. V., and Lin, Y.-C.: Characterization of the sources and processes of organic and inorganic aerosols in New York city with a high-resolution time-of-flight aerosol mass apectrometer, Atmos. Chem. Phys., 11, 1581–1602, doi:10.5194/acp-11-1581-2011, 2011.
Trebs, I., Meixner, F. X., Slanina, J., Otjes, R., Jongejan, P., and Andreae, M. O.: Real-time measurements of ammonia, acidic trace gases and water-soluble inorganic aerosol species

ACPD
15, 35117–35155, 2015

at a rural site in the Amazon Basin, Atmos. Chem. Phys., 4, 967–987, doi:10.5194/acp-4-967-2004, 2004.
Ulbrich, I. M., Canagaratna, M. R., Zhang, Q., Worsnop, D. R., and Jimenez, J. L.: Interpretation of organic components from Positive Matrix Factorization of aerosol mass spectrometric data, Atmos. Chem. Phys., 9, 2891–2918, doi:10.5194/acp-9-2891-2009, 2009.
Ulden, A. P. and Wieringa, J.: Atmospheric boundary layer research at Cabauw, Bound.-Lay. Meteorol., 78, 39–69, 1996.
Varga, B., Kiss, G., Ganszky, I., Gelencsar, A., and Krivacsy, Z.: Isolation of water-soluble organic matter from atmospheric aerosol, Talanta, 55, 561–572, 2001.
Vermeulen, A. T., Hensen, A., Popa, M. E., van den Bulk, W. C. M., and Jongejan, P. A. C.: Greenhouse gas observations from Cabauw Tall Tower (1992–2010), Atmos. Meas. Tech., 4, 617–644, doi:10.5194/amt-4-617-2011, 2011.
WHO: WHO Air quality guidelines for particulate matter, ozone, nitrogen dioxide and sulfur dioxide, World Health Organization, 20 Avenue Appia, 1211 Geneva, 27, Switzerland, 2006.
WHO: Burden of disease from Household Air Pollution for, 2012: World Health Organization (WHO), available at: http://www.who.int/phe/health_topics/outdoorair/databases/en/, last access: 12 June 2014.
Zhang, Q., Jimenez, J. L., Canagaratna, M. R., Ulbrich, I. M., Ng, N. L., Worsnop, D. R., and Sun, Y.: Understanding atmospheric organic aerosols via factor analysis of aerosol mass spectrometry: a review, Anal. Bioanal. Chem., 401, 3045–3067, 2011.
Zhang, Y. and Wu, S.-Y.: Fine scale modeling of agricultural air quality over the southeastern United States using two air quality models. Part II. Sensitivity studies and policy implications, Aerosol Air Qual. Res., 13, 1475–1491, 2013.

Table 1. Results of the ACSM to MARGA and ACSM to AMS comparisons for individual species and the respective total masses. Note that for comparison with the MARGA total mass concentrations, only the ACSM inorganic species were considered.

		Slope	intercept $\mu g\, m^{-3}$	R^2
Chl	MARGA	0.49 ± 0.02	0.11 ± 0.01	0.24
	AMS	0.67 ± 0.01	-0.01 ± 0.01	0.31
NH_4	MARGA	0.88 ± 0.01	0.07 ± 0.01	0.93
	AMS	0.82 ± 0.03	0.01 ± 0.02	0.71
SO_4	MARGA	0.63 ± 0.01	-0.08 ± 0.01	0.86
	AMS	0.49 ± 0.02	-0.18 ± 0.02	0.76
NO_3	MARGA	1.23 ± 0.01	-0.37 ± 0.03	0.96
	AMS	1.17 ± 0.02	-0.04 ± 0.02	0.89
Organics	AMS	1.03 ± 0.04	0.07 ± 0.04	0.73
Total	MARGA	1.05 ± 0.01	-0.70 ± 0.06	0.93
	AMS	0.90 ± 0.02	-0.02 ± 0.07	0.84

ACPD
15, 35117–35155, 2015

Aerosol source apportionment from 1 year measurements at the CESAR tower at Cabauw, NL

P. Schlag et al.

Title Page
Abstract Introduction
Conclusions References
Tables Figures
◂◂ ▸▸
◂ ▸
Back Close
Full Screen / Esc
Printer-friendly Version
Interactive Discussion

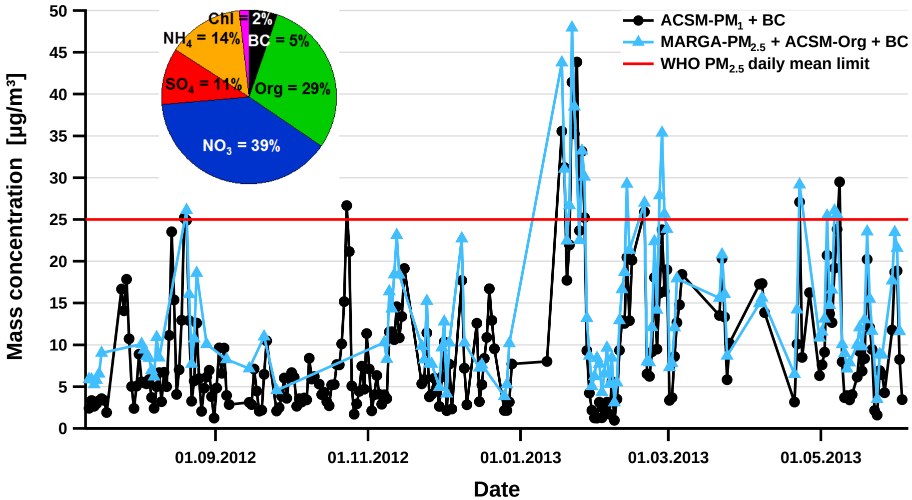

Figure 1. Time series of the daily mean. The black line represents the sum of BC and all ACSM species, the blue line the sum of BC, ACSM organics and all MARGA-$PM_{2.5}$ species. The pie chart shows the fractional abundances of individual BC and ACSM species averaged over the whole campaign. Missing BC data was filled with zero values, thus deriving lower concentration limits.

ACPD
15, 35117–35155, 2015

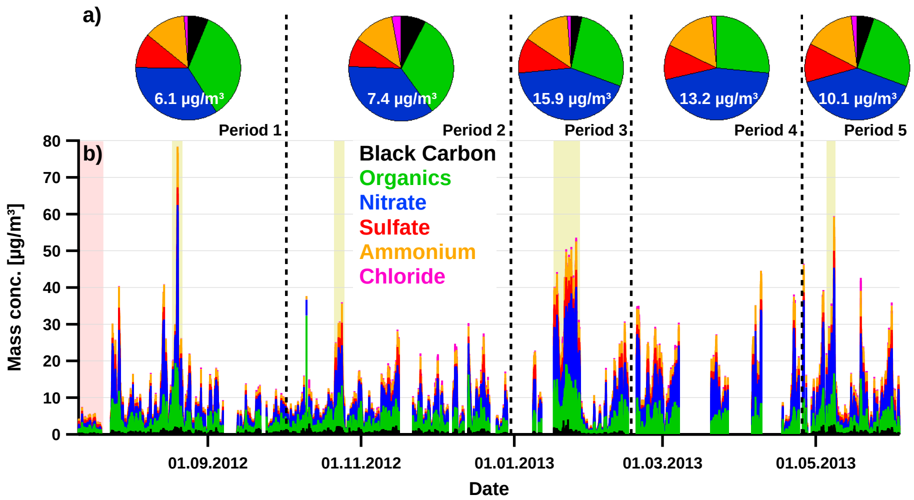

Figure 2. Overview of the ACSM campaign: **(a)** pie charts of average fractional abundances of aerosol species, separated in five periods. The respective average total mass concentration is written inside the pie chart. **(b)** Stacked time series of mass concentrations of aerosol species. The temporal overlap with the AMS is highlighted in red. Pollution events are indicated by green shaded areas.

ACPD
15, 35117–35155, 2015

Aerosol source apportionment from 1 year measurements at the CESAR tower at Cabauw, NL

P. Schlag et al.

Title Page
Abstract Introduction
Conclusions References
Tables Figures
◀| |▶
◀ ▶
Back Close
Full Screen / Esc
Printer-friendly Version
Interactive Discussion

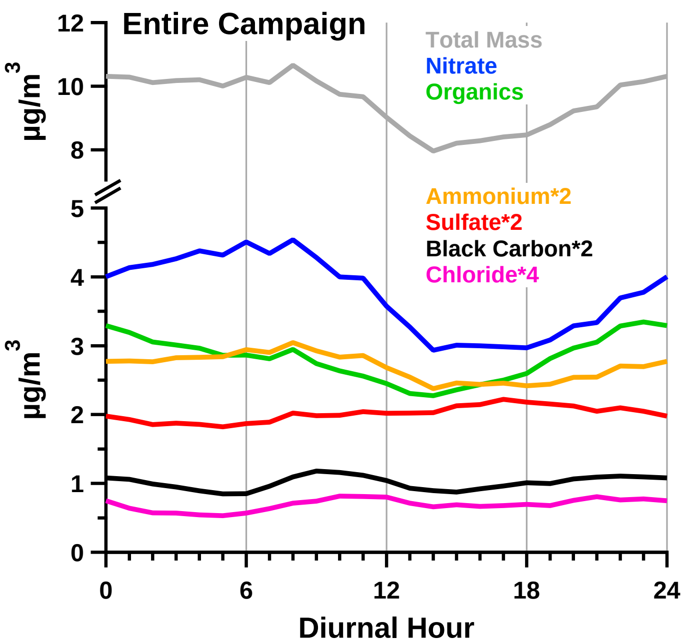

Figure 3. Diurnal variation (local time, LT) of individual species and the total mass, averaged over the whole ACSM campaign

ACPD
15, 35117–35155, 2015

Aerosol source apportionment from 1 year measurements at the CESAR tower at Cabauw, NL

P. Schlag et al.

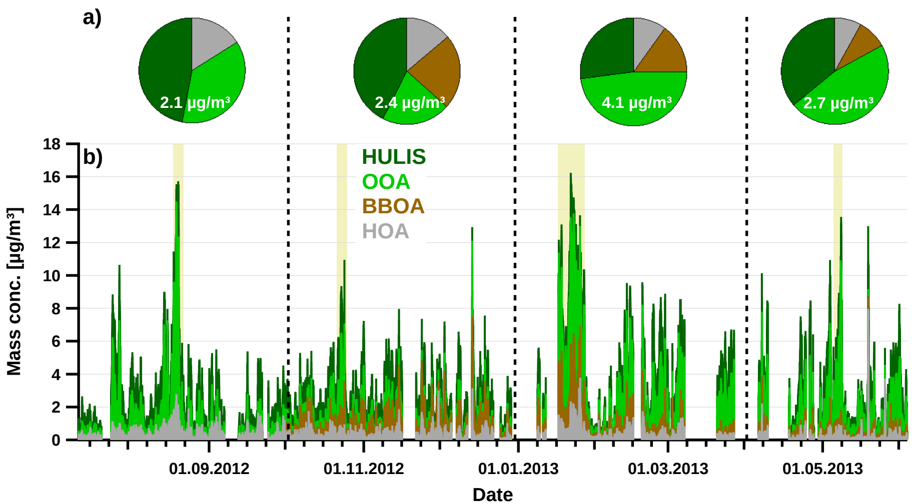

Figure 4. Overview of ACSM PMF factors: **(a)** seasonal pie charts of the factor contributions. The respective average total organic concentration is written inside the pie chart. **(b)** Stacked time series of mass concentrations. Green shaded areas represent highly polluted events.

ACPD
15, 35117–35155, 2015

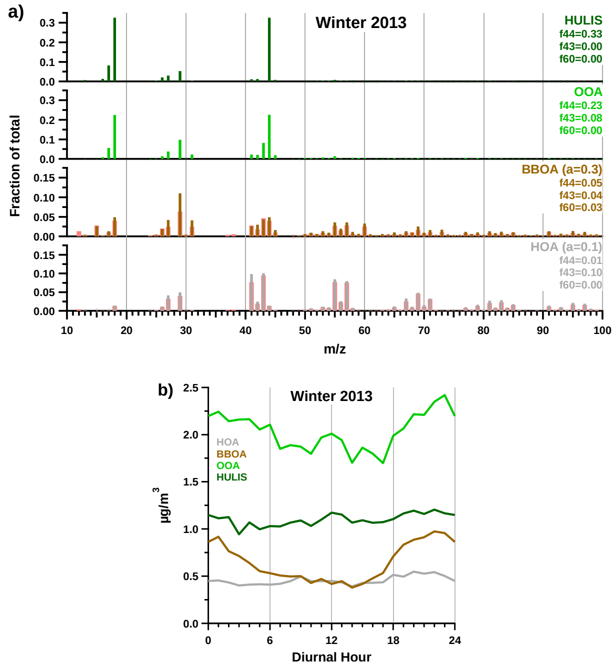

Figure 5. (a) Mass spectra of ACSM PMF factors and **(b)** average diurnal variations (LT) of ACSM factors found in Winter 2013. For the constrained profiles HOA and BBOA, the applied *a* value is written in brackets. Corresponding reference spectra are shown by red bars. Note that the *y* axis scales of the POA profiles are zoomed by a factor of 2 comparing to SOA profiles.

ACPD
15, 35117–35155, 2015

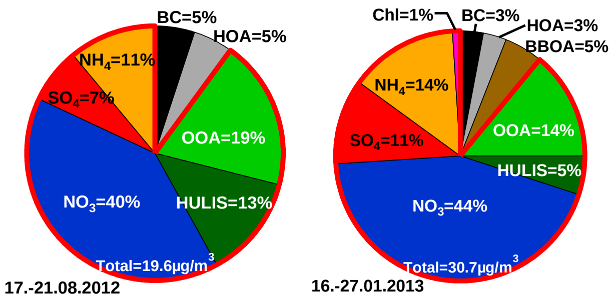

Figure 6. Average contributions of individual aerosol species and PMF factors during selected pollution events. Surrounded red regions represent the secondary aerosol fraction.

ACPD
15, 35117–35155, 2015

Aerosol source apportionment from 1 year measurements at the CESAR tower at Cabauw, NL

P. Schlag et al.